Acta Biochim Biophys Sin 2023, 55(10): 1561–1570
https://doi.org/10.3724/abbs.2023126
Advance Access Publication Date: 28 August 2023
Original Article

Original Article

WDR38, a novel equatorial segment protein, interacts with the GTPase protein RAB19 and Golgi protein GM130 to play roles in acrosome biogenesis

Qiujie Gao[1,2], Gang Liu[3], Lihua Huang[1], Yunfei Zhang[1,2], Xinxing Zhang[1,2], Xiaoyue Song[1,2], and Xiaowei Xing[1,*]

[1]Center for Experimental Medicine, Third Xiangya Hospital, Central South University, Changsha 410013, China, [2]Department of Laboratory Medicine, Third Xiangya Hospital, Central South University, Changsha 410013, China, and [3]The Institute of Reproduction and Stem Cell Engineering, School of Basic Medical Sciences, Central South University, Changsha 410078, China
*Correspondence address. Tel: +86-13975806774; E-mail: davy2222@163.com

Received 13 December 2022 Accepted 14 April 2023

Abstract

The WD40-repeat containing (WDR) proteins are enriched in the testis and play important roles in spermatogenesis. In the present study, we investigate the expression profile of WDR38, a novel member of the WDR protein family, in humans and mice. RT-qPCR (reverse transcription-quantitative polymerase chain reaction) results demonstrate that WDR38 mRNA is abundantly expressed in both the human and mouse testis. The expression of mouse Wdr38 is strictly regulated during development. Further immunofluorescence staining results show that WDR38 is located in the equatorial segment of the acrosome in human and mouse mature spermatozoa and is involved in acrosome biogenesis. Subcellular localization analysis reveals that the mouse Wdr38 protein is distributed in the perinuclear cytoplasm of transfected cells and colocalizes with the GTPase protein Rab19 and Golgi protein GM130. Coimmunoprecipitation (co-IP) assays demonstrate that Wdr38, Rab19 and GM130 interact with each other in the mouse testis and in HEK293T cells. In acrosome biogenesis, Wdr38, Rab19 and GM130 aggregate at the nuclear membrane to form large vesicles, and GM130 then detaches and moves towards the caudal region of the nucleus, whereas the Wdr38/Rab19 complex spreads along the dorsal nuclear edge and finally docks to the equatorial segment. These results indicate that WDR38 is a novel equatorial segment protein that interacts with the GTPase protein RAB19 and Golgi protein GM130 to play roles in acrosome biogenesis.

Key words WDR38, RAB19, GM130, acrosome biogenesis, equatorial segment

Introduction

Infertility is a highly prevalent reproductive health condition affecting 8%–12% of couples of the reproductive-age population worldwide [1]. In China, 25% of couples who were actively trying to become pregnant experienced the problem of infertility [2]. Approximately 50% of cases of infertility are due to male factors [3]. There are many factors causing male infertility, among which genetic factors are very important for spermatogenesis. To date, over 2000 genes associated with spermatogenesis have been identified, and loss of function of these genes leads to spermatogenesis failure and male infertility [3].

Emerging evidence has indicated that WD40-repeat (WDR)-containing proteins, such as WDR12, WDR42A, WDR52, WDR62, WDR63, WDR66 and WDR96, are involved in the process of spermatogenesis [4–11]. The WD40-repeat was first identified in the β-subunit of the heterotrimeric GTP-binding protein (G protein) [12]. Typical WDR proteins are characterized by a sequence repeat of 40-60 amino acids that ends in a tryptophan (W)–aspartate (D) dipeptide [13]. To explore the function of the WDR62 protein, Qin *et al.* [8] constructed *Wdr62*-knockout mice and found that these male mice were completely infertile. Further study revealed that Wdr62 is involved in spindle assembly by interacting with the centrosome-associated protein Cep170 in spermatogenesis. In contrast to WDR62, the WDR proteins WDR12 and WDR42A (also called

DCAF8) were reported to be associated with the head formation in spermatozoa [4,5]. Homozygous mutation of *WDR12* resulted in tapered-head spermatozoa in humans, while deficiency of *Wdr42a* resulted in bent head malformations in more than 40% of spermatids in male mice. However, numerous WDR proteins, including WDR52 (also called cilia and flagella associated protein CFAP44), WDR63, WDR66 and WDR96 (also called CFAP43), have been identified to be associated with multiple morphological abnormalities of sperm flagella (MMAF) [6,7,9,10]. Lu *et al.* [9] showed that Wdr63 interacts with Wdr78, which is necessary for inner dynein arm assembly. *Wdr63*-knockout in mice leads to a reduced sperm number, abnormal flagella and male infertility. These data suggest that WDR proteins play critical and unique roles in male fertility.

WDR38 is a member of the WD40 protein family; it contains 315 amino acid residues and 7 WD40-domain repeats (40 amino acid residues per repeat), with a molecular weight of 34 kDa. In a previous study, Djureinovic *et al.* [14] performed a genome-wide transcriptomic analysis in the human testis and demonstrated that *WDR38* expression is enhanced in the testis, with an increase in mRNA expression of at least 4-fold compared to the average level in all other tissues. Recently, we searched the single-cell RNA sequencing database and found that the expression of human and mouse *WDR38* mRNA is detected in all stages from spermatogonia to elongating spermatids in spermatogenesis, indicating that WDR38 may participate in spermatogenesis (Supplementary Figure S1) [15,16].

In a previous study, Fukuda *et al.* [17] carried out a yeast two-hybrid assay with 28 different mouse or human Rab proteins (Ras-related proteins, Rab1-30) as bait to systematically screen for Rab effectors and found that Wdr38 might interact with Rab19. Rab19 belongs to the Rab family, which includes well-known key regulators in steps of intracellular membrane trafficking, such as vesicle docking, trafficking and fusion [18]. Rab proteins usually interact with GM130 to regulate vesicle transport and fusion [19]. Valsdottir *et al.* [20] found that Rab33b binds to GM130 to regulate vesicle docking of the endoplasmic reticulum to *cis*-Golgi transport *in vitro*.

GM130 was first isolated from the Golgi matrix as a structural protein and localized to the cis-side of the Golgi apparatus [21]. Han *et al.* [22] demonstrated that inactivation of GM130 caused the absence of acrosomes and male infertility. In their study, they established *GM130*-knockout mice and found that *GM130*-deficiency in mice did not affect the secretion of proacrosomal vesicles, but the vesicles failed to fuse and could not form a large acrosomal vesicle, eventually leading to acrosome deletion. Considering the dynamic source, Rab19 plays a potential role in binding with GM130, and Wdr38 contains a coiled β-propeller architecture and may be a possible effector of Rab19 [17]. Thus, we speculate that Wdr38, Rab19 and GM130 may interact and participate in the process of vesicle trafficking and fusion in spermatogenesis.

In the present study, we investigated the expression profile, cellular localization, subcellular localization of WDR38, as well as its interaction with RAB19 and GM130 to elucidate its biological functions and mechanism in spermatogenesis.

Materials and Methods

Animals

C57BL/6J mice were obtained from the Department of Laboratory Animals of Central South University and were maintained according to approved guidelines (Guidelines for the Care and Use of Laboratory Animals). All animal experiments were approved by the Ethics Committee of the Department of Laboratory Animals, Central South University (CSU20220509) and were performed according to laboratory animal management practices.

Human samples

Human surgical tissues (testis, spleen, fat, muscle, colon, and liver) and peripheral blood samples were collected for RNA extraction. This study was approved by the Ethics Committee of Third Xiangya Hospital, Central South University (No. 22231), and all subjects signed informed consent forms. Human sperm smears were preserved in our laboratory [23].

Bioinformatics analysis

Multiple sequence alignment of WDR38 in different species and phylogenetic analysis of WDR38, WDR9, WDR12, WDR19, WDR42A, WDR52, WDR62, WDR63, WDR66 and WDR96 were performed using Clustal Omega (https://www.ebi.ac.uk/Tools/msa/clustalo/). The crystal structure of human WDR38 was predicted by Phyre2 (http://www.sbg.bio.ic.ac.uk/phyre2/html/). The distribution of human WDR38 protein in cells was predicted by online data from the Human Protein Atlas (https://www.proteinatlas.org/). The expression of *WDR38* in testicular germ cells was analyzed with previously published human and mouse single-cell RNA sequencing data. The subcellular localization of the WDR38 protein in humans was predicted by the PSORT prediction tool (https://psort.hgc.jp/).

RT-qPCR

RNA was isolated from human and mouse tissues using Trizol reagent (Invitrogen, Carlsbad, USA) according to the manufacturer's protocol. First-strand cDNA was synthesized with HiScript II Q RT SuperMix (Vazyme, Nanjing, China) for qPCR. qPCR was performed on a Light Cycler 480 Real Time PCR instrument (Roche, Basel, Switzerland). The qPCR cycle conditions were as follows: 1 cycle of pre-denaturation at 95°C for 30 s, and 40 cycles of denaturing at 95°C for 10 s, annealing and extension at 60°C for 30 s, followed by temperature-ramping dissociation steps (95°C for 15 s, 60°C for 60 s, and 95°C for 15 s) for melting curve. Primer sequences are listed in Supplementary Table S1. Each experiment was performed in three replicate wells and repeated at least three times. Relative expression levels of target genes were analysed by the $2^{-\Delta\Delta Ct}$ method. The housekeeping gene *GAPDH* was used as a control.

Immunohistochemical staining

Paraffin sections of mouse testis were deparaffinized and hydrated. Citric acid antigen retrieval buffer (Biosharp, Hefei, China) was used to perform antigen retrieval. Endogenous peroxidase activity was quenched with 3% hydrogen peroxide for 10 min at room temperature. After being blocked with 5% BSA at room temperature or 30 min, the sections were incubated with anti-WDR38 antibody (Supplementary Table S2) at 4°C overnight and then incubated with peroxidase-conjugated goat anti-rabbit secondary antibody (Servicebio, Wuhan, China). The sections were subsequently stained using DAB (Servicebio) and counterstained with Harris haematoxylin (Servicebio). Finally, specific signals were observed under an LSM 780 multiphoton microscope (Carl Zeiss, Oberkochen, Germany).

Construction of expression plasmids

To construct the plasmid pLVX-IRES-Puro-*Wdr38*-Flag, the ORF

(open reading frame) of *Wdr38* was amplified from mouse testis (C57BL/6J) by RT-qPCR. PCR products were purified and digested with the restriction enzymes *Eco*RI and *Bam*HI (Invitrogen). After separation by gel electrophoresis, the target bands were excised, and the DNA was purified using a Gel Purification Kit (Axygen, Carlsbad, USA) following the manufacturer's protocol. Finally, the fragment was inserted into pLVX-IRES-Puro (Honorgene, Changsha, China) and sequenced. To construct the plasmids pEGFP-N1-*Wdr38* and pEGFP-N1-*Rab19*, we amplified the ORFs of *Wdr38* and *Rab19* from mouse testis (C57BL/6J) by RT-PCR. The purified *Wdr38* and *Rab19* PCR products were digested with the restriction enzymes *Hin*dIII and *Sal*I (Invitrogen), respectively. Subsequently, the target fragments were inserted into pEGFP-N1 (Clontech, Mountain View, USA). The accuracy of the inserted fragments was confirmed by DNA sequencing. The primers used to construct these plasmids are listed in Supplementary Table S1.

Cell culture and transfection

HEK293T cells were purchased from the American Type Culture Collection (ATCC, Manassas, USA) and were cultured in 2 mL of Dulbecco's modified Eagle's medium (Gibco, Carlsbad, USA) supplemented with 10% fetal bovine serum (Gibco) at 37°C under 5% CO_2. Cover slips were placed at the bottom of each well of six-well plates. HEK293T cells were transiently transfected with 2.5 μg of the pEGFP-N1-*Wdr38* plasmid with 3.5 μL of Lipo8000™ solution (Beyotime, Shanghai, China) and cultured for 48 h. Forty-eight hours later, cells on coverslips were fixed with 4% paraformaldehyde (PFA) and stained with DAPI (Beyotime). Finally, fluorescence was observed under the LSM 780 multiphoton microscope.

Immunofluorescence assay

The immunofluorescence assay was performed as previously described [24]. Briefly, the slides were washed with 0.1% Triton X-100 in PBS (hereafter PBS-T) 3 times and permeabilized with 0.5% Triton X-100 for 15 min. Subsequently, the slides were blocked with 5% BSA for 1 h at room temperature and incubated with primary antibodies at 4°C overnight. After three 5-min washes with PBS-T, the slides were incubated with the corresponding secondary antibodies at room temperature for 1 h. Rhodamine-PNA (Rhodamine-Labelled Peanut Agglutinin; Vector Laboratories, Newark, USA) was used to stain the acrosomes of spermatids and spermatozoa. Finally, 4′,6-diamidino-2-phenylindole (DAPI; Beyotime) was used to stain the nuclei, and fluorescence was observed using the LSM 780 multiphoton microscope. The antibodies used are listed in Supplementary Table S2. The experiment was repeated at least three times independently.

Western blot analysis

Testicular tissues and HEK293T cells were suspended in RIPA lysis buffer (Biosharp) with phenylmethanesulfonyl fluoride (PMSF; Biosharp) and incubated for 20 min on ice. The lysate was centrifuged at 13,400 *g* for 30 min at 4°C. Then, proteins were separated on 10%–12% SDS-PAGE and subsequently transferred onto a polyvinylidene fluoride (PVDF) membrane (Millipore, Billerica, USA). After blocking the membrane with 5% non-fat dried milk in TBS-T at room temperture (RT) for 1 h, the primary antibody (Supplementary Table S2) was added, and the membrane was incubated at 4°C overnight. Then, the membrane was washed three times with TBS-T and incubated with secondary antibodies for 1 h at RT, followed by washing for 3 times. An Enhanced chemiluminescence kit (Biosharp) was used to visualize the protein bands with a UVP Chem Studio PLUS multifunctional imager (Analytik Jena, Berlin, Germany).

Coimmunoprecipitation assay

The plasmids pLVX-IRES-Puro-Flag-*Wdr38* and pEGFP-N1-*Rab19* (7.5 μg of each plasmid) were cotransfected into HEK293T cells. HEK293T cells or testicular tissues were lysed with 1 mL of IP lysis buffer (Invitrogen) containing a protease inhibitor mixture (Glpbio, Montclair, USA) at 4°C for 15 min, and the lysates were centrifuged to obtain the supernatant. The supernatant was incubated with targeted antibodies or a mock antibody, and incubated with rotation at 4°C overnight. Subsequently, 30 μL of Protein A/G-coated magnetic beads (Invitrogen) was added for conjugation to the antibody complexes. The immune complexes were eluted and neutralized for subsequent western blot analysis. Western blot analysis was performed as described above. The antibodies used are listed in Supplementary Table S2. The experiment was repeated at least three times.

Statistical analysis

For comparison of gene expression in testis versus other tissues and gene expression in testis at different developmental stages, one-way ANOVA followed by a Fisher's protected least significant difference test was performed using GraphPad PRISM version 8. The significance level was set at $P < 0.05$.

Results

Bioinformatics analysis of WDR38

To understand the characteristics of WDR38, the WDR38 amino acid sequences of different species were aligned by Clustal Omega, and the results showed that the WDR38 protein sequence is evolutionarily highly conserved among humans, mice, rats, chimpanzees, monkeys, cattle and pigs (Figure 1A). Furthermore, we compared the WDR38 amino acid sequence with those of other WDR proteins that have been reported to be involved in spermatogenesis, such as WDR96, WDR66, WDR63, WDR62, WDR52, WDR42A, WDR38, WDR19, WDR12, and WDR9. The phylogenetic data suggested that WDR38 and WDR12 may share a common origin (Figure 1B). Recently, Hua *et al.* [4] demonstrated that WDR12 is a novel protein associated with tapered-head sperm and male infertility. Thus, we suggested that the function of WDR38 is probably similar to that of WDR12 and that WDR38 plays important roles in the spermatozoa head. Moreover, we used Phyre2 software to analyze the three-dimensional structure of human WDR38 and found that it has the typical characteristics of WD40 proteins, with a coiled β-propeller architecture containing seven WD40 blades (Figure 1C).

WDR38 is highly expressed in human and mouse testes

In previous studies, Mistry *et al.* [13] found that 60%–73% of WD40 genes were highly expressed in mouse and human testes. To investigate the expression profile of *WDR38* in humans, we amplified *WDR38* cDNA from testicular, fat, colon, muscle, spleen, and liver tissues and peripheral blood by RT-qPCR and found that *WDR38* was expressed in all samples, with the highest expression in the testis (Figure 2A). In addition, we measured *Wdr38* mRNA expression in different tissues of mice by RT-qPCR, and the results also showed that *Wdr38* is abundant in the testis and weakly expressed in the ovary, small intestine, brain, muscle, heart, liver,

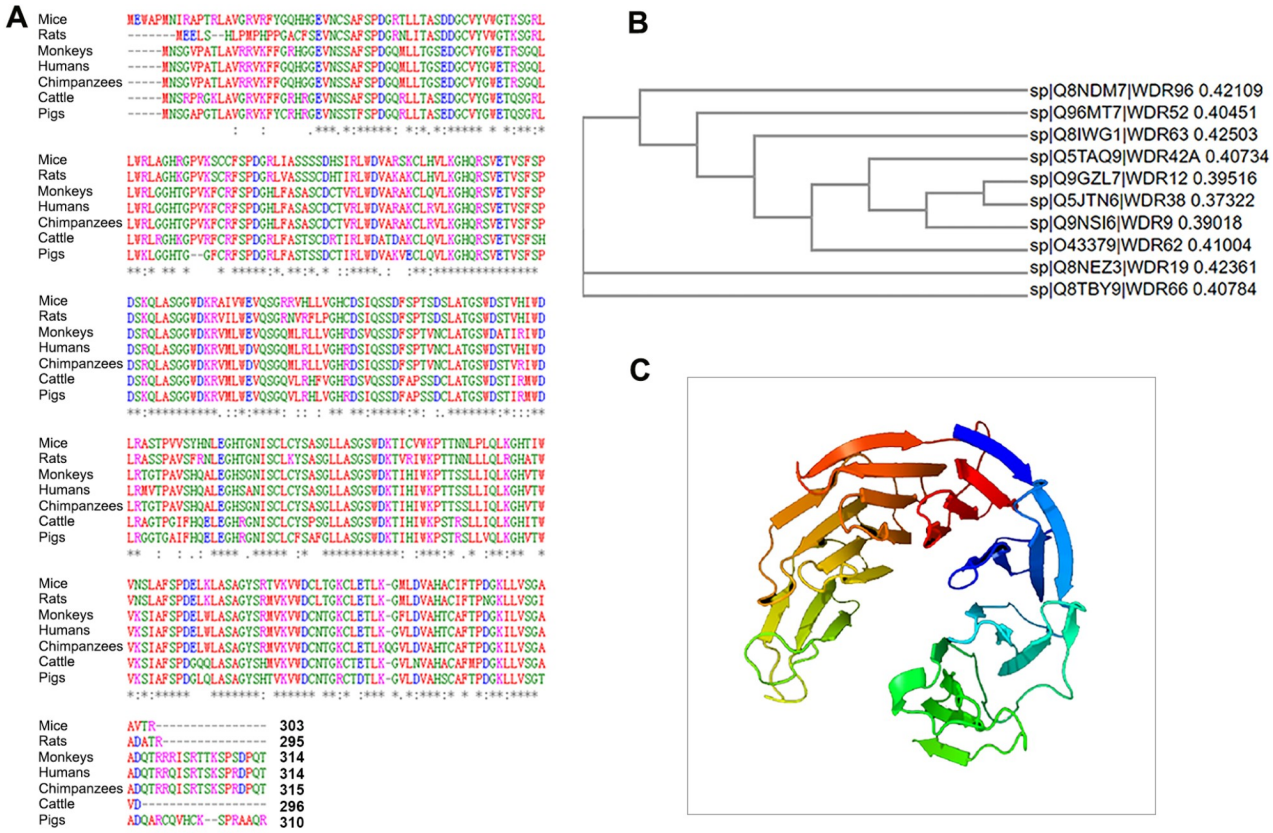

Figure 1. Bioinformatics analysis of the WDR38 protein (A) Homology analysis of the amino acid sequence of WDR38 showed that it is highly conserved among mice (AAI15630.1), rats (NP_001386264.1), monkeys (NP_001180625.2), humans (AAI71828.1), chimpanzees (PNI69332.1), cattle (AAI49695.2) and pigs (XP_020924282.1) using Clustal Omega (https://www.ebi.ac.uk/Tools/msa/clustalo/). The asterisks indicate matching sequences in different species. (B) Phylogenetic tree analysis of WD40 proteins associated with spermatogenesis showed that human WDR38 and WDR12 probably originated from a close common ancestor. (C) Three-dimensional structure of WDR38 predicted with the web-based Phyre2 portal. The different colors represent the seven WD40 blades.

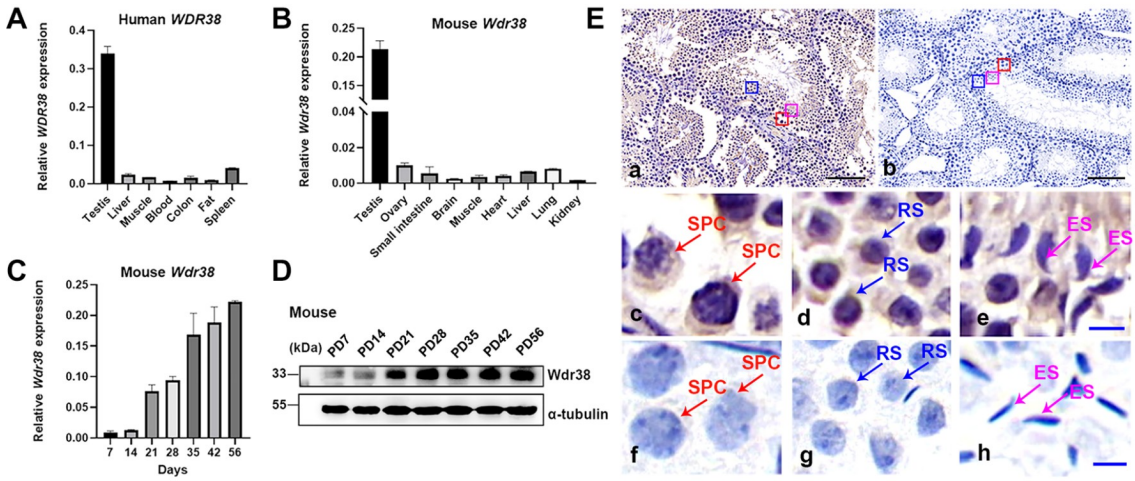

Figure 2. Expression pattern of WDR38 in human and mouse tissues (A) The expression of *WDR38* in human testicular, fat, colon, muscle, spleen, and liver tissues and peripheral blood was measured by RT-qPCR (mean ± SD, $n = 3$). (B) The expression of *Wdr38* in the mouse testis, ovary, small intestine, brain, muscle, heart, liver, lung and kidney was measured by RT-qPCR (mean ± SD, $n = 3$). (C) The expression of *Wdr38* in different developmental stages of the mouse testis was measured by RT-qPCR (mean ± SD, $n = 3$). (D) Western blot analysis of Wdr38 protein expression at different developmental stages of the mouse testis. α-Tubulin was used as a loading control. PD, postnatal day. (E) Immunohistochemical analysis of the localization of Wdr38 in the adult mouse testis. Brown staining, indicating a positive signal, was detected in spermatocytes (SPC, red arrows) and round spermatids (RS, blue arrows) and in the head of elongating spermatids (ES, pink arrows). No significant brown staining was detected in the slide processed with the negative control (b,f–h). Scale bar: 100 μm (a,b), 5 μm (c–h).

lung and kidney (Figure 2B). Furthermore, to discover the temporal expression of *Wdr38*, we performed RT-qPCR at different developmental stages of the mouse testis and found that *Wdr38* mRNA was expressed in the testes of 7-day-old mice, exhibited a significant increase in expression from postnatal day 21 and continued to exhibit a high expression level in the adult mouse testis (Figure 2C). The trend of change in its protein level is similar to that in its mRNA level (Figure 2D), indicating that *Wdr38* is strictly regulated by development.

To observe the distribution of the Wdr38 protein, immunohistochemical staining was performed to detect Wdr38 in 8-week-old mouse testis (Figure 2E). Brown staining, indicating positive signals, was detected in the cytoplasm of spermatocytes (SPC) (Figure 2E, c) and round spermatids (RS) (Figure 2E, d) and in the head of elongating spermatids (ES) (Figure 2E, e). No obvious positive signals were observed in slides processed with the negative control (Figure 2E, b,f–h). These results suggested that Wdr38 may be involved in spermatogenesis.

WDR38 localizes to the equatorial segment of mature spermatozoa and participates in acrosome formation

To further understand the distribution of WDR38 during spermatogenesis, we carried out immunostaining of WDR38 in mature spermatozoa, and the results demonstrated that in both human and mouse spermatozoa, WDR38 was localized in the equatorial segment (Figure 3A). Subsequently, we investigated the dynamic distribution of Wdr38 in mouse germ cells by immunofluorescence staining. The results showed that green fluorescence-labelled Wdr38 was present as granule-like structures in the cytoplasm of spermatogonia, primary spermatocytes and secondary spermatocytes. In round spermatids, we observed that Wdr38 moved to one side of the nucleus and then aggregated into a large vesicular structure covering the nucleus. As the sperm head and acrosome elongated, Wdr38 spread along the dorsal edges of nuclei and finally localized in the acrosomal region of spermatozoa (Figure 3B). This result indicated that Wdr38 is involved in acrosome biogenesis.

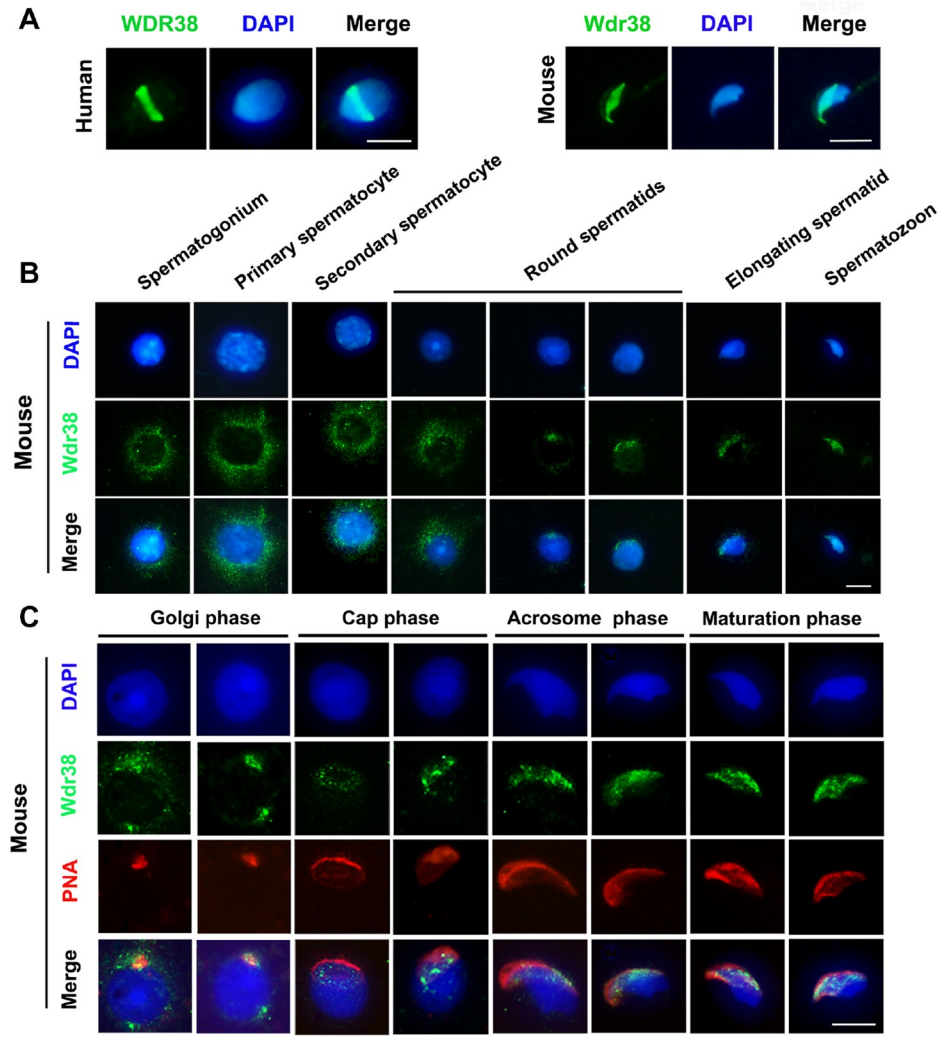

Figure 3. The dynamic expression of Wdr38 in different spermatogenic cells was analyzed by immunofluorescence analysis (A) WDR38 localized to the equatorial segment (ES) in mature spermatozoa of humans (left panel) and mice (right panel), as determined using indirect immunofluorescence. Nuclei were stained with DAPI (blue). Scale bar: 5 μm. (B) Immunofluorescence staining revealed that Wdr38 is expressed during spermatogenesis from spermatogonia to spermatids in mouse testicular cells. Nuclei were stained with DAPI (blue). Scale bars: 5 μm. (C) The colocalization of Wdr38 and PNA during acrosome biogenesis was visualized by immunofluorescence staining. The acrosomes of spermatids were labelled with PNA (red), and nuclei were stained with DAPI (blue). Scale bars: 5 μm. The experiment was repeated three times independently with similar results (A–C).

Acrosome biogenesis is divided into four successive phases: the Golgi, cap, acrosome and maturation phases. To obtain detailed information, we further used peanut agglutinin (PNA) to stain the acrosome and examined the precise distribution of Wdr38 during acrosome biogenesis by double-immunofluorescence staining. As shown in Figure 3C, the results revealed that at the Golgi stage, red fluorescence-labelled PNA-positive small vesicles accumulated in the cytoplasm of spermatid nuclei, green fluorescence-labelled granule-like Wdr38 was clustered on one side in the perinuclear cytoplasm, and PNA was colocalized with Wdr38. During the cap phase, the PNA signal covered the nucleus like a cap, and the Wdr38 signal was distributed under the PNA signal and partially overlapped with the PNA signal. At the acrosome stage, the Wdr38 signal was encircled by the PNA signal at the dorsal edge of nucleus. Compared with that of the PNA signal, the localization of the Wdr38 signal was closer to the inner side of the spermatid nucleus. Finally, Wdr38 retained its localization to the equatorial segment of the acrosome in the maturation phase. These data suggested that as an equatorial segment protein, Wdr38 is involved in acrosome biogenesis.

Wdr38 interacts with Rab19 in the Golgi apparatus

To determine the localization of WDR38 in cells, we predicted the subcellular localization of human WDR38 by different online software programs, and the results showed that WDR38 is distributed in the cytoplasm (https://psort.hgc.jp/). By searching the Human Protein Atlas Database, we found that WDR38 is possibly localized to vesicles (https://www.proteinatlas.org/). To confirm these data experimentally, we constructed the recombinant plasmid pEGFP-N1-*Wdr38* and transiently transfected it into HEK293T cells, and the results are shown in Figure 4A. Green

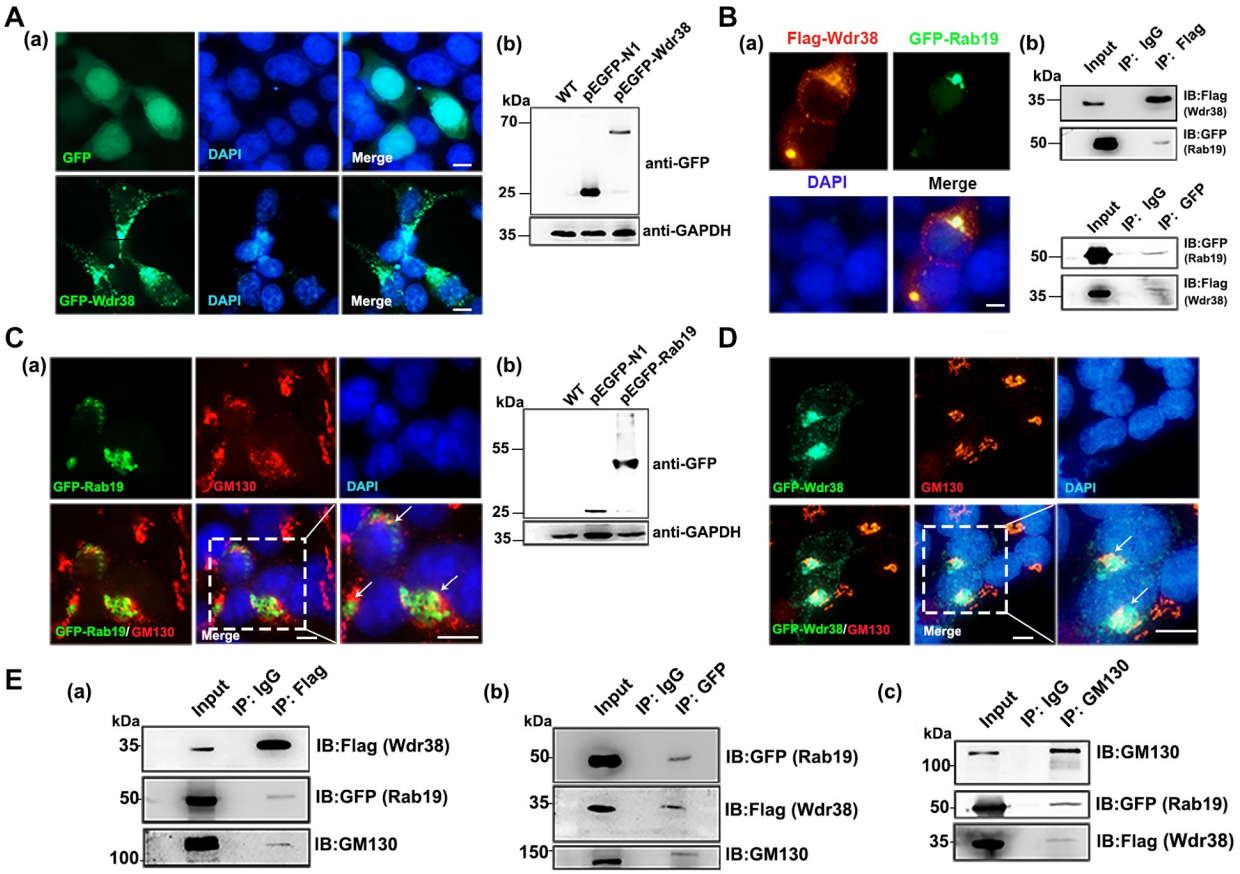

Figure 4. GM130 interacts with the Wdr38/Rab19 complex *in vitro* (A) HEK293T cells were transfected with pEGFP-N1 and pEGFP-Wdr38. The immunofluorescence results showed that the green fluorescence-labelled Wdr38 fusion protein mainly accumulated in the perinuclear cytoplasm; however, green fluorescence was distributed throughout HEK293T cells transfected with pEGFP-N1 (a). Nuclei were stained with DAPI (blue). Scale bar: 5 μm. Western blot analysis revealed that the pEGFP-Wdr38 fusion protein was expressed in HEK293T cells (b). GAPDH was used as a loading control. (B) The immunofluorescence results showed that Flag-Wdr38 colocalized with GFP-Rab19 in HEK293T cells transfected with pEGFP-*Rab19* and pLVX-IRES-Puro-Flag-*Wdr38* recombinant plasmids (a). Nuclei were stained with DAPI (blue). The interaction between Wdr38 and Rab19 was verified *in vitro* by co-IP assays in HEK293T cells transfected with pEGFP-*Rab19* and pLVX-IRES-Puro-Flag-*Wdr38* recombinant plasmids (b). (C) The immunofluorescence results showed that Rab19 colocalized with GM130 in HEK293T cells transfected with the pEGFP-*Rab19* recombinant plasmid. Higher magnification images of the boxed areas are shown on the right, and the colocalization of Rab19 and GM130 is indicated with white arrows (a). Nuclei were stained with DAPI (blue). Scale bar: 5 μm. Western blot analysis revealed that the pEGFP-Rab19 fusion protein was expressed in HEK293T cells (b). GAPDH was used as a loading control. (D) The immunofluorescence results showed that Wdr38 colocalized with GM130 in HEK293T cells transfected with the pEGFP-*Wdr38* recombinant plasmid. Higher magnification images of the boxed areas are shown on the right, and the colocalization of Wdr38 and GM130 is indicated with white arrows. Nuclei were stained with DAPI (blue). Scale bar: 5 μm. (E) The interaction of Wdr38, Rab19 and GM130 was verified *in vitro* by co-IP assay in HEK293T cells transfected with the pEGFP-*Rab19* and pLVX-IRES-Puro-Flag-*Wdr38* recombinant plasmids. Forty-eight hours after transfection, cells were collected for reciprocal immunoprecipitation (IP) with an anti-Flag (Wdr38) antibody (a), anti-GFP (Rab19) antibody (b) and anti-GM130 antibody (c), and the precipitates were analyzed with anti-GFP, anti-Flag or GM130 antibodies. The experiment was repeated three times independently with similar results (A–E).

fluorescence was distributed throughout HEK293T cells transfected with pEGFP-N1. However, the green fluorescence-labelled Wdr38 fusion protein mainly accumulated in the perinuclear cytoplasm, and there were multiple granule-like structures in the cytoplasm. The expression of the fusion protein GFP-Wdr38 was confirmed by western blot analysis.

Previously, Fukuda e*t al.* [17] reported that Wdr38 is a potential effector of Rab19 and Sinka *et al.* [25] demonstrated that Rab19 interacts with Golgin-97 and localizes to the Golgi apparatus in the secondary cells of *Drosophila*. In this study, we cotransfected pLVX-IRES-Puro-Flag-*Wdr38* and pEGFP-N1-*Rab19* into HEK293T cells. As shown in Figure 4B, red fluorescence-labelled Wdr38 and green fluorescence-labelled Rab19 colocalized in the Golgi apparatus. Further co-IP analysis indicated that the Wdr38 protein was pulled down by the anti-Flag antibody, and the Rab19 protein was also pulled down by the anti-GFP antibody. Rab19 was present in the Flag-Wdr38 immunoprecipitate. In the reciprocal co-IP assay, Wdr38 was detected in the GFP-tagged Rab19 immunoprecipitate, suggesting that Wdr38 interacts with Rab19 *in vitro*.

GM130 binds to the Wdr38/Rab19 complex *in vitro*

GM130 (also named Golgin A2) is a *cis*-Golgi tethering protein that interacts with Rab proteins for Golgi transport [19]. Moyer *et al.* [26] demonstrated that GM130 binds to Rab1 to form the Rab1-GM130 complex to regulate COPII-Golgi transport. Valsdottir *et al.* [20] provided evidence that GM130 binds to Rab33b to regulate vesicle transport to the *cis*-Golgi apparatus. Thus, we speculated that Rab19 may also interact with GM130. To verify this, we introduced pEGFP-N1-*Rab19* into HEK293T cells, and the expression of the fusion protein Rab19-GFP was confirmed by western blot analysis. The colocalization of Rab19 and GM130 was analyzed by immunostaining, and the results showed that green fluorescence-labelled Rab19 colocalized with red fluorescence-labelled GM130 (Figure 4C). We also found that Wdr38 colocalized with GM130 at the large vesicle (Figure 4D). Furthermore, we performed a co-IP assay using anti-Flag, anti-GFP and anti-GM130 antibodies. The results showed that Wdr38, Rab19 and GM130 were detected in all immunoprecipitates (Figure 4E), indicating that Wdr38, Rab19 and GM130 might interact with each other *in vitro*.

Wdr38, Rab19 and GM130 interact with each other in the mouse testis

To explore whether Wdr38 interacts with Rab19 and GM130 in the mouse testis, we isolated mouse testicular proteins and performed co-IP assay using anti-Wdr38, anti-Rab19 and anti-GM130 antibodies, and the results showed that Wdr38, Rab19 and GM130 could interact with each other (Figure 5A). We also examined the localization of Wdr38 and Rab19 in mouse and human mature

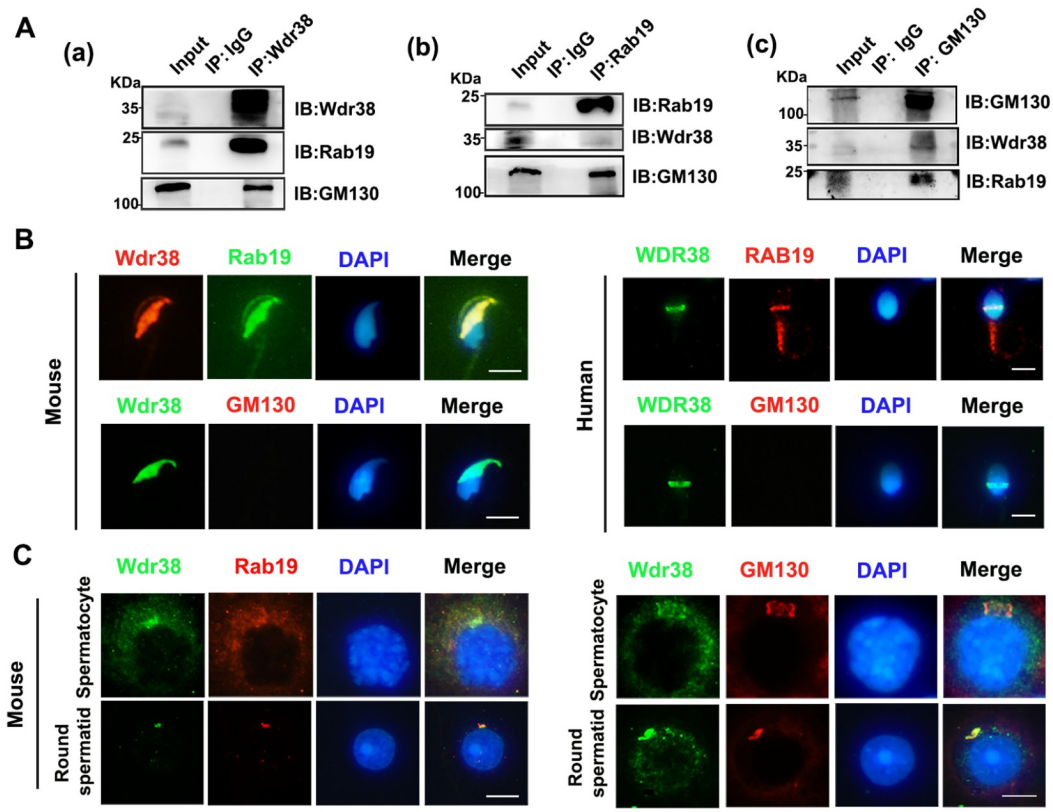

Figure 5. Wdr38 interacts with Rab19 and GM130 to participate in acrosome biogenesis (A) A co-IP assay was performed to analyze the interaction of Wdr38, Rab19 and GM130 in the mouse testis. The mouse testicular proteins were collected for reciprocal immunoprecipitation (IP) with an anti-Flag (Wdr38) antibody (a), anti-GFP (Rab19) antibody (b) and anti-GM130 antibody (c), and the precipitates were analyzed with anti-Wdr38, anti-Rab19 or GM130 antibodies. (B) WDR38 colocalized with RAB19 in human and mouse mature spermatozoa, as determined by immunofluorescence analysis; however, GM130 was not detected in mature spermatozoa in humans and mice. Nuclei were stained with DAPI (blue). Scale bar: 5 μm. (C) Spermatocytes and round spermatids were subjected to immunofluorescence staining with anti-Wdr38, anti-Rab19 and anti-GM130 antibodies as indicated. GM130 is a *cis*-Golgi marker. Scale bar: 5 μm. The experiment was repeated three times independently with similar results (A–C).

spermatozoa by double immunofluorescence staining. The results showed that mouse Rab19 was detected in the equatorial segment and the tail of mature spermatozoa and was colocalized with Wdr38 at the equatorial segment (Figure 5B). Similar results were also obtained in human spermatozoa (Figure 5B). However, GM130 expression was deficient in both mouse and human spermatozoa (Figure 5B). We performed immunostaining assays in spermatocytes and round spermatids, and the results showed that Wdr38 was colocalized with Rab19 and GM130 in stages of spermatogenesis (Figure 5C).

The interaction among Wdr38, Rab19 and GM130 plays roles in acrosome biogenesis

The acrosome is a unique membranous organelle that is derived from vesicles secreted by the *trans*-Golgi apparatus. Acrosome biogenesis begins at the early stage of spermiogenesis and proceeds through four successive phases (Golgi phase, cap phase, acrosome phase, and maturation phase) [27]. We observed that Wdr38 and Rab19 were colocalized in spermatocytes, round spermatids and elongated spermatids. In the Golgi phase, both Wdr38 and Rab19 accumulated in the concave region of the nuclear surface to form a large vesicle (Figure 6A). Stenmark *et al.* [18] concluded that the Rab family plays an important role in vesicle transport and fusion. We suggest that Rab19 and Wdr38 promote vesicle fusion and regulate vesicle-directed transport to the acrosome during acrosomal biogenesis by recruiting vesicles derived from the Golgi apparatus.

In the Golgi phase, Wdr38 and GM130 colocalized in the large vesicle. From the late Golgi phase, GM130 detached from the Wdr38/Rab19 complex, migrated to the caudal region, and disappeared at maturation phase of acrosome biogenesis (Figure 6B), consistent with the lack of GM130 expression in mature spermatozoa (Figure 5B). GM130, as a vesicular tethering factor, is involved in the assembly and fusion of proacrosomal vesicles in germ cells. In *GM130*-knockout mice, the secretion of proacrosomal vesicles was not affected, but the vesicles failed to fuse and could not form a large acrosomal vesicle [22]. We speculated that the

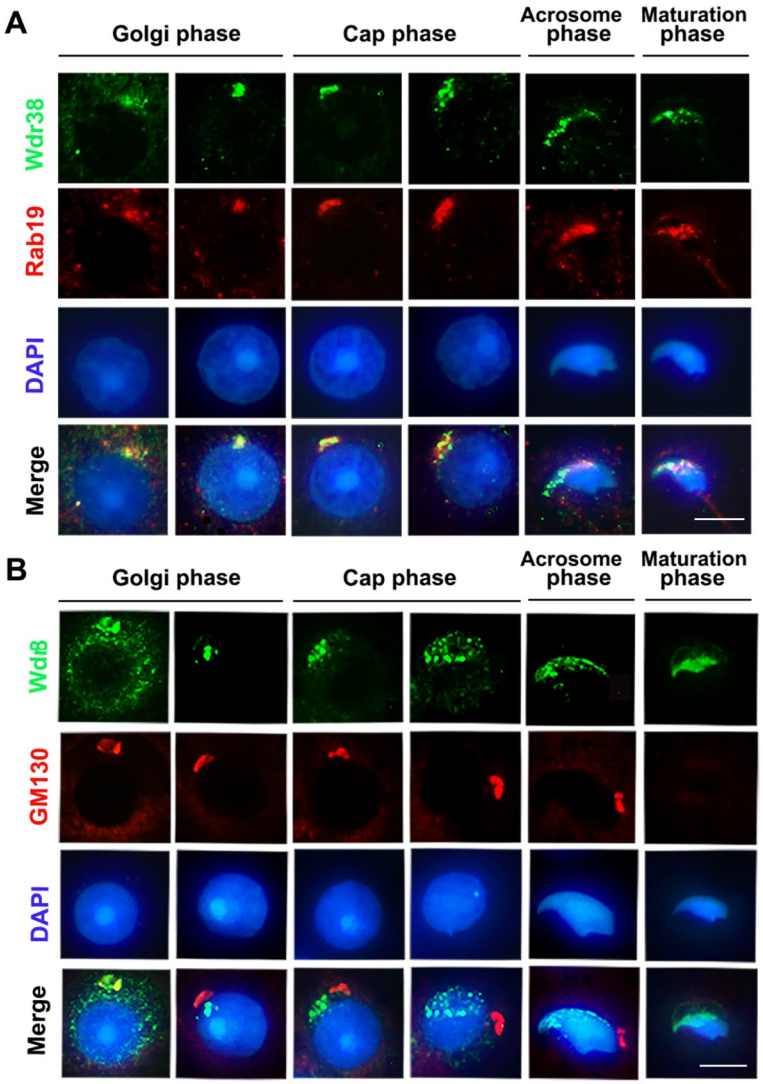

Figure 6. The dynamic expression of Wdr38, Rab19 and GM130 in acrosome biogenesis evaluated by immunofluorescence analysis
(A) Immunofluorescence staining of Wdr38 and Rab19 during acrosome biogenesis using mouse testicular cell smears. Scale bar: 5 μm. (B) Immunofluorescence staining of Wdr38 and GM130 (Golgi apparatus) during acrosome biogenesis using mouse testicular cell smears. Scale bar: 5 μm. The experiment was repeated three times independently with similar results (A,B).

Wdr38/Rab19 complex docks to the vesicle and that GM130 may mediate the fusion of the vesicle with the nucleus by interacting with the Wdr38/Rab19 complex.

From the cap phase, the Wdr38/Rab19 complex spread along the dorsal edge of the nucleus, similar to a "cap" covering the nucleus, and gradually migrated to the equatorial segment in mouse spermatozoa in the maturation phase (Figure 6A). These data indicated that Wdr38 is involved in acrosome biogenesis by interacting with Rab19 and GM130.

Discussion

WD40 family genes are highly expressed in the testes of mice and humans [13]. Recently, Mistry *et al.* [13] studied the expressions of WD40 family genes (such as *Wdr12*, *Wdr51b*, *Wdr53*, etc.) by RT-qPCR and found that these genes were abundantly expressed in the mouse testis. In this study, we investigated the expression profile of *WDR38* and found that its mRNA expression was also enriched in the testis in both humans and mice, and we demonstrated that the expression of *Wdr38* was regulated by development in mice. In addition, the immunohistochemical staining results showed that Wdr38 was distributed in spermatocytes, round spermatids and elongating spermatids, consistent with the single-cell RNA sequencing results in the mouse testis.

Recent studies have revealed that WD40 repeat proteins are involved in spermatogenesis. WD40 repeat proteins such as WDR52, WDR63, WDR66 and WDR96 are associated with spermatozoon flagellum [6,7,9,10]. Dysfunction of these proteins lead to MMAF. Hua *et al.* [4] demonstrated that unlike the above mentioned proteins, WDR12 downregulation induced by mutation of the *WDR12* gene is associated with tapered-head sperm and male infertility. Through bioinformatics analysis, we found that WDR38 and WDR12 have the closest genetic distance; thus, we speculated that WDR38 may play a role in head shaping. In the present study, we demonstrated by immunofluorescence staining that WDR38 resides in the equatorial segment of mature sperm in humans and mice.

To explore the molecular mechanism of Wdr38, we analyzed the subcellular localization of mouse Wdr38 and found that Wdr38 localized to the Golgi apparatus, where it colocalized with the Golgi protein Rab19 and the Golgi marker GM130, suggesting that Wdr38 is a Golgi-associated protein. Further co-IP assays confirmed that Wdr38, Rab19 and GM130 interact with each other and form the Wdr38/Rab19/GM130 complex, which is localized at the Golgi apparatus *in vitro*. Since the Golgi apparatus in spermatids is involved in acrosome biogenesis during spermatogenesis, we investigated the dynamic distribution of the complex in the process of spermatogenesis and found that the Wdr38/Rab19 and Wdr38/GM130 complexes were detected in the perinuclear area of spermatocytes and in the large vesicles of round spermatids in the Golgi phase. At the cap phase, GM130 detached from the Wdr38/Rab19 complex, moved to the caudal region, and was not detected at the maturation phase. The Wdr38/Rab19 complex spread along the dorsal nucleus in spermatids and gradually localized to the equatorial segment at the maturation phase. In the process of vesicle transport to the sperm nucleus, we speculated that Wdr38 is docked in the Golgi apparatus, which is an effector of Rab19, and is recruited to the surface of the Golgi apparatus by interacting with Rab19. Then, the binding of the Wdr38/Rab19 complex to the tethering factor GM130 may promote the coating, fusion and anchoring of vesicles on the sperm nucleus. After the acrosomal vesicle fused with the nuclear membrane, GM130 dissociated from the Wdr38/Rab19 complex. We observed that in the acrosome phase, the PNA signal covered the outer layer of the nucleus, while the Wdr38 signal was near the nucleus and moved to the equatorial segment at the maturation phase.

Recent studies have revealed that equatorial segment proteins are involved in acrosome biogenesis. It was found that SPACA1 is localized on the equatorial segment of the acrosome. *SPACA1* deficiency in male mice produces round-headed sperm; in many of these spermatids, after step 8 of acrosome biogenesis, the acrosome begins to degenerate and disappear, resulting in male infertility [28]. Wolkowicz *et al.* [29] demonstrated that the equatorial segment protein SPESP1 is involved in acrosome biogenesis. The SPESP1 protein was first detected in the proacrosomal granules of Golgi-phase round spermatids. In spermatids with flattened acrosomal vesicles, SPESP1 is concentrated at the vesicle periphery. With acrosome development to the cap and elongation phases, SPESP1 remains in the acrosomal vesicle, migrates posteriorly along the nuclear envelope and finally docks at the equatorial segment. In our study, we found that Wdr38, as an equatorial segment protein, is also involved in acrosome biogenesis. Thus, we suggest that equatorial segment proteins play an important role in acrosome biogenesis.

In summary, we first reported that Wdr38, as a novel equatorial segment protein, interacts with Rab19 and GM130 to participate in acrosome biogenesis. Wdr38 acts as an effector of Rab19, and Rab19 promotes the fusion and transport of proacrosomal vesicles through recruitment of Wdr38. GM130 interacts with Wdr38 and Rab19 to participate in the fusion of vesicles and the anchoring of the acrosome to the sperm nucleus. Our findings will aid in understanding the function of *WDR38* and the molecular mechanism of spermatogenesis.

Supplementary Data

Supplementary data is available at *Acta Biochimica et Biophysica Sinica* online.

Acknowledgement

We would like to thank Xiyi He and Shuting Zhang (Center for Experimental Medicine, Third Xiangya Hospital of Central South University, Changsha, China) for their help in cell culture.

Funding

This work was supported by the grants from the Clinical Medical Technology Innovation Guidance Project of Hunan Province (No. 2021SK53716) and the Graduate Student Independent Exploration Innovation Fund of Central South University (No. 1053320215836).

Conflict of Interest

The authors declare that they have no conflict of interest.

References

1. Agarwal A, Baskaran S, Parekh N, Cho CL, Henkel R, Vij S, Arafa M, *et al.* Male infertility. *Lancet* 2021, 397: 319–333
2. Zhou Z, Zheng D, Wu H, Li R, Xu S, Kang Y, Cao Y, *et al.* Epidemiology of infertility in China: a population-based study. *BJOG* 2018, 125: 432–441
3. Krausz C, Riera-Escamilla A. Monogenic forms of male infertility. *Exp Suppl* 2019, 111: 341–366
4. Hua J, Guo L, Yao Y, Hu W, Wan YY, Xu B. Biallelic mutations in WDR12 are associated with male infertility with tapered-head sperm. *Asian J*

Androl 2022, 24: 1–6
5. Zhang X, Xia Z, Lv X, Li D, Liu M, Zhang R, Ji T, *et al.* DDB1- and CUL4-associated factor 8 plays a critical role in spermatogenesis. *Front Med* 2021, 15: 302–312
6. Tang S, Wang X, Li W, Yang X, Li Z, Liu W, Li C, *et al.* Biallelic mutations in CFAP43 and CFAP44 cause male infertility with multiple morphological abnormalities of the sperm flagella. *Am J Hum Genet* 2017, 100: 854–864
7. Coutton C, Vargas AS, Amiri-Yekta A, Kherraf ZE, Ben Mustapha SF, Le Tanno P, Wambergue-Legrand C, *et al.* Mutations in CFAP43 and CFAP44 cause male infertility and flagellum defects in Trypanosoma and human. *Nat Commun* 2018, 9: 686
8. Qin Y, Zhou Y, Shen Z, Xu B, Chen M, Li Y, Chen M, *et al.* WDR62 is involved in spindle assembly by interacting with CEP170 in spermatogenesis. *Development* 2019, 146: dev174128
9. Lu S, Gu Y, Wu Y, Yang S, Li C, Meng L, Yuan W, *et al.* Bi-allelic variants in human WDR63 cause male infertility via abnormal inner dynein arms assembly. *Cell Discov* 2021, 7: 110
10. Kherraf ZE, Amiri-Yekta A, Dacheux D, Karaouzène T, Coutton C, Christou-Kent M, Martinez G, *et al.* A homozygous ancestral SVA-insertion-mediated deletion in WDR66 induces multiple morphological abnormalities of the sperm flagellum and male infertility. *Am J Hum Genet* 2018, 103: 400–412
11. Auguste Y, Delague V, Desvignes JP, Longepied G, Gnisci A, Besnier P, Levy N, *et al.* Loss of calmodulin- and radial-spoke-associated complex protein CFAP251 leads to immotile spermatozoa lacking mitochondria and infertility in men. *Am J Hum Genet* 2018, 103: 413–420
12. Fong HK, Hurley JB, Hopkins RS, Miake-Lye R, Johnson MS, Doolittle RF, Simon MI. Repetitive segmental structure of the transducin beta subunit: homology with the CDC4 gene and identification of related mRNAs. *Proc Natl Acad Sci USA* 1986, 83: 2162–2166
13. Mistry BV, Alanazi M, Fitwi H, Al-Harazi O, Rajab M, Altorbag A, Almohanna F, *et al.* Expression profiling of WD40 family genes including DDB1- and CUL4-associated factor (DCAF) genes in mice and human suggests important regulatory roles in testicular development and spermatogenesis. *BMC Genomics* 2020, 21: 602
14. Djureinovic D, Fagerberg L, Hallström B, Danielsson A, Lindskog C, Uhlén M, Pontén F. The human testis-specific proteome defined by transcriptomics and antibody-based profiling. *Mol Hum Reprod* 2014, 20: 476–488
15. Hermann BP, Cheng K, Singh A, Roa-De La Cruz L, Mutoji KN, Chen IC, Gildersleeve H, *et al.* The mammalian spermatogenesis single-cell transcriptome, from spermatogonial stem cells to spermatids. *Cell Rep* 2018, 25: 1650–1667.e8
16. Wang M, Liu X, Chang G, Chen Y, An G, Yan L, Gao S, *et al.* Single-cell RNA sequencing analysis reveals sequential cell fate transition during human spermatogenesis. *Cell Stem Cell* 2018, 23: 599–614.e4
17. Fukuda M, Kanno E, Ishibashi K, Itoh T. Large scale screening for novel rab effectors reveals unexpected broad rab binding specificity. *Mol Cell Proteomics* 2008, 7: 1031–1042
18. Stenmark H. Rab GTPases as coordinators of vesicle traffic. *Nat Rev Mol Cell Biol* 2009, 10: 513–525
19. Nakamura N. Emerging new roles of GM130, a cis-Golgi matrix protein, in higher order cell functions. *J Pharmacol Sci* 2010, 112: 255–264
20. Valsdottir R, Hashimoto H, Ashman K, Koda T, Storrie B, Nilsson T. Identification of rabaptin-5, rabex-5, and GM130 as putative effectors of rab33b, a regulator of retrograde traffic between the Golgi apparatus and ER. *FEBS Lett* 2001, 508: 201–209
21. Nakamura N, Rabouille C, Watson R, Nilsson T, Hui N, Slusarewicz P, Kreis TE, *et al.* Characterization of a cis-Golgi matrix protein, GM130. *J Cell Biol* 1995, 131: 1715–1726
22. Han F, Liu C, Zhang L, Chen M, Zhou Y, Qin Y, Wang Y, *et al.* Globozoospermia and lack of acrosome formation in GM130-deficient mice. *Cell Death Dis* 2018, 8: e2532
23. Liu G, Xing X, Zhang H, Zhu W, Lin G, Lu G, Li W. Patients with acephalic spermatozoa syndrome linked to novel *TSGA10/PMFBP1* variants have favorable pregnancy outcomes from intracytoplasmic sperm injection. *Clin Genet* 2021, 100: 334–339
24. Li X, Wu Y, Huang L, Yang L, Xing X. SPAG4L/SPAG4L interacts with Nesprin2 to participate in the meiosis of spermatogenesis. *Acta Biochim Biophys Sin* 2019, 51: 669–676
25. Sinka R, Gillingham AK, Kondylis V, Munro S. Golgi coiled-coil proteins contain multiple binding sites for Rab family G proteins. *J Cell Biol* 2008, 183: 607–615
26. Moyer BD, Allan BB, Balch WE. Rab1 interaction with a GM130 effector complex regulates COPII vesicle *cis*-Golgi tethering. *Traffic* 2001, 2: 268–276
27. Xiong W, Shen C, Wang Z. The molecular mechanisms underlying acrosome biogenesis elucidated by gene-manipulated mice. *Biol Reprod* 2021, 105: 789–807
28. Fujihara Y, Satouh Y, Inoue N, Isotani A, Ikawa M, Okabe M. SPACA1-deficient male mice are infertile with abnormally shaped sperm heads reminiscent of globozoospermia. *Development* 2012, 139: 3583–3589
29. Wolkowicz MJ, Shetty J, Westbrook A, Klotz K, Jayes F, Mandal A, Flickinger CJ, *et al.* Equatorial segment protein defines a discrete acrosomal subcompartment persisting throughout acrosomal biogenesis. *Biol Reprod* 2003, 69: 735–745